Energy-time-entangled two-photon molecular absorption

D. Tabakaev, M. Montagnese, G. Haack, L. Bonacina ⊙, J.-P. Wolf ⊙, H. Zbinden, and R. T. Thew ⊙

Département de Physique Appliquée, Université de Genève, 1211 Genève, Switzerland

Nonlinear spectroscopy and microscopy techniques are ubiquitous in a wide range of applications across physics and biology. However, these usually rely on high-powered pulsed laser systems. A promising alternative is to exploit entangled two-photon absorption (ETPA), which can lead to tens of orders of magnitude lower incident fluxes than in conventional two-photon absorption schemes. However, the role of different entangled degrees of freedom in ETPA was unclear following recent experimental studies, when compared to earlier theoretical works. Here, we first demonstrate a linear dependence of the ETPA rate with the photon-pair rate, a clear signature of ETPA, and estimate the values for the concentration-dependent ETPA cross section for Rhodamine 6G. We then investigate the signature of energy-time entanglement and polarization dependence in the ETPA fluorescence rate and demonstrate a strong dependence of the signal on the interphoton delay that reflects the coherence time of the entangled two-photon wave packet.

I. INTRODUCTION

Building on Marie Göppert-Mayer's discovery of two-photon absorption (TPA), nonlinear spectroscopic techniques have become invaluable tools for both fundamental and applied research, providing the opportunity to study atomic and molecular transition levels that would be unattainable with linear spectroscopy [1]. However, these techniques typically use relatively high peak power pico- or femtosecond pulsed lasers to compensate for the low probability of two photons arriving simultaneously at the same atom or molecule [2,3].

A promising solution to address this photo-sensitive limitation is to exploit the concept of entangled two-photon absorption (ETPA) [4]. Consider a simple model for two-photon absorption [4] where one photon excites an absorbing specimen from the ground state (g) to a virtual level and the other photon further excites this to the final state (f), as illustrated in the energy level diagram on the right of Fig. 1. In the case of classical TPA, the absorption rate of two photons is a product of two independent single-photon absorption rates, resulting in a quadratic dependence on the photon flux ϕ, $R_c = \delta_r \phi^2$ [1/s] [4–6]. Here, δ_r is the classical TPA cross section in units of cm^4 s. However, if the photons are produced in the form of entangled pairs, they act more like a single object, resulting in a linear absorption rate, $R_e = \sigma_e \phi_{\text{pair}}$ [1/s], where ϕ_{pair} is now the photon-pair flux—a photon-pair rate per unit area—and σ_e[cm^2] is the ETPA cross section [4]. We can then write the overall two-photon absorption rate as $R_2 = \delta_r \phi^2 + \sigma_e \phi_{\text{pair}}$.

The linear dependence of the absorption rate on the photon-pair rate is a signature that the process is due to ETPA [4,6–13]. The ETPA process dominates at low flux, before the classical, quadratic, TPA takes over at $\phi_{\text{pair}} = \phi = \sigma_e/\delta_r$. To give an idea of the advantage provided by ETPA in terms of the required flux, the typical values for classical TPA are around $\delta_r \sim 10^{-47}$ cm^{4}s [14], while for ETPA, values as high

as $\sigma_e \sim 10^{-17}$ cm^2 have been obtained for certain molecules [8,9,11].

Motivated by this, there have been numerous theoretical studies to develop spectroscopic techniques based on ETPA to investigate a wide range of molecular systems [7]. If we consider the energy-level diagram on the right of Fig. 1, in the case of TPA, the transition from the ground state is due to absorption of two photons with bandwidths Δ_1 and Δ_2, which are comparable in value to the bandwidth of the final state Δ_f [for Rhodamine 6G (Rh6G)]. In contrast, due to the energy-time entanglement, the ETPA transition behaves like it is induced by a spontaneous parametric down-conversion (SPDC) pump photon with bandwidth $\Delta_p \ll \Delta_f$, similarly to single-photon absorption (SPA).

Recently, experiments have started to explore this concept, primarily looking at the linear dependence of ETPA with respect to the photon pair rate [8–13,15]. While the original theoretical works [4,5] and other experiments [16–18] focused on energy-time entanglement [19], some of these recent experiments emphasized the role of polarization entanglement [10,13,15,20] or did not distinguish which degree of freedom is entangled. In this work we investigate this situation by analyzing the ETPA-induced fluorescence intensity of Rh6G with respect to different degrees of freedom of the pairs. This choice for the molecule is motivated by strong absorption properties of Rh6G in the desired wavelength range 510–540 nm and its high quantum yield [21]. The measurements we performed allow us to demonstrate that the correlations due to energy-time entanglement provide the fundamental advantage for ETPA.

II. EXPERIMENTAL SETUP

The experimental setup is based on a periodically poled lithium niobate (PPLN) Type-0 SPDC source for generating entangled photon pairs and three different elements as shown
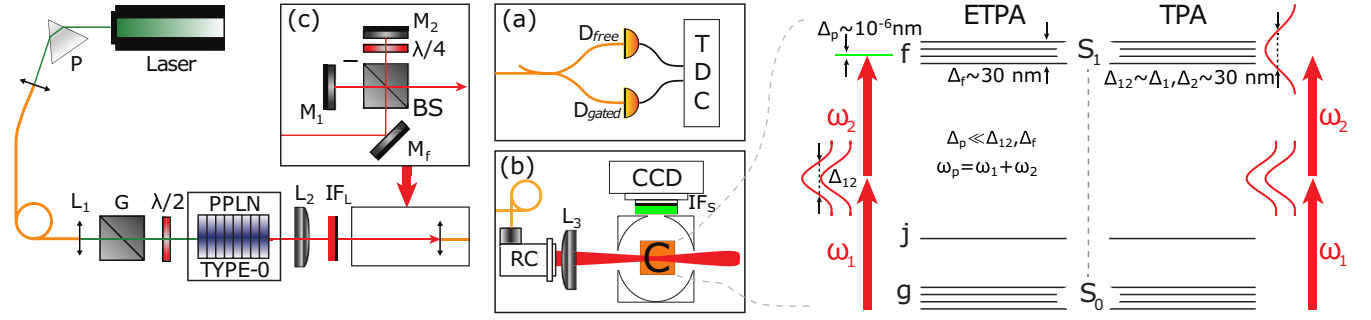
FIG. 1. Experimental schematic: A 532 nm laser beam (Coherent Verdi V5) was sent through a prism (P), coupled to a single-mode fiber, and focused to a 230 μm waist by an 11 mm focal length lens L_1 inside a 2 cm Type-0 quasi-phase-matched PPLN crystal, producing SPDC pairs, which are then collimated by a 20 cm focal length lens L_2. A Glan prism (G) and wave plate ($\lambda/2$) were used to ensure linearity of the pump polarization before the crystal. To remove any residual 532 nm pump photons, two long-pass interference filters (IF$_L$) (Thorlabs FELH0750) were used. The photon coincidence counting setup (a) consists of a 50:50 fiber beamsplitter, free-running single-photon detector (D_{free}) (ID Quantique ID220), gated single-photon detector (D_{gated}) (ID Quantique ID201), and a time-to-digital converter (TDC) (ID Quantique ID801). In panel (b), the pairs were coupled to a fiber, passed through a reflective collimator (RC), and focused by a 20 cm focal length lens L_3 (10 cm for the free-space setup) into an integrating sphere (Thorlabs IS236A-4) containing a custom-made cuvette filled with the Rh6G solution. The counts were collected with a CCD camera (Atik 383L+) attached to one of the integrating sphere's ports. A short-pass filter (IF$_S$) (Thorlabs FESH0650) was installed before the camera to further reduce spurious detection events. Pairs sent to the interferometer (c) were separated on the beamsplitter (BS), to introduce either a delay ($\Delta\tau$) or a polarization rotation ($\lambda/4$ waveplate) between the photons. The figure on the right represents the energy level diagram of the absorbing specimen and the various bandwidths for ETPA and TPA regimes.

in Fig. 1(a)–1(c)]. This type of source allows us to avoid any ambiguity about the nature of ETPA by minimizing the entangled degrees of freedom. This photon-pair source also allows us to improve the photon-pair rate, and hence to have a greater measurement dynamic compared to previous studies [9,10,13].

Calibration of the pair-source is done by sending the pairs to a standard coincidence detection scheme comprising two single-photon detectors and a time-to-digital converter [Fig. 1(a)]. We measured an average coincidence detection rate of 1100 s^{-1} at 5.1 mW of pump power. Taking into account losses, the beamsplitter, and the detection efficiencies of around 3% at 1064 nm, this corresponds to around $2.6 \times 10^6 \text{ s}^{-1}$ fiber-coupled pairs. This calibration was made in a low rate regime to avoid saturating the detectors.

Once the calibration was done, the SPDC pairs were sent to the fluorescence detection setup [Fig. 1(b)], where they were focused (60 μm waist) into the cuvette containing the Rh6G molecules in an ethanol solution. The cuvette was placed inside a 2 inch integrating sphere, with a (17.6 mm × 13.52 mm sensor) CCD camera attached to one of its 1/2 inch ports, to maximize collection and detection of SPDC-induced fluorescence. Another port of the sphere was left open, opposite the input, to allow the unabsorbed pairs to pass through minimizing the chances of spurious detection events due to residual 1064 nm photons, which is further reduced by a short-pass filter installed before the camera.

The role of energy-time entanglement in the ETPA-induced fluorescence was investigated by inserting a Michelson interferometer before the fluorescence detection setup as shown in Fig. 1(c). In one arm of the interferometer a variable path length can be controlled to introduce a delay between the photons, and hence, the arrival time difference of the photons sent to the cuvette. Additionally, a $\lambda/4$ waveplate is introduced in one path of the interferometer to rotate the polarization of

one photon with respect to the other to test any polarization dependence of the input state.

III. ETPA LINEARITY AND CROSS SECTION

The measurement of the ETPA-induced fluorescence dependence on the photon pair rate represents the first step to demonstrate the linear signature of ETPA. The combination of an integrating sphere and camera was used to improve the collection efficiency; however, the large camera sensor area also introduces a high background noise rate.

To calibrate them, a series of measurements were made to quantify all contributions to the detected signal (see Fig. 2 for typical values). To obtain the true signal we extracted the background camera counts from measurements with a sample of pure ethanol (N_E) from those with Rh6G (N_{PM}). These measurements were repeated for each data run and concentration. Importantly, we also ensured that there were no events due to leakage of the 532 nm pump (N_{NPM}), which, due to its high single-photon-absorption cross section, would also produce a linear response to pump power. This was achieved by tuning the temperature away from the phase-matching condition, such that no pairs were produced. To further check the absence of the 532 nm pump leakage, the output of the fiber was connected to a single-photon detector (ID Quantique ID 100) where only detector dark counts were observed even at maximum pump power. N_D corresponds to the camera's dark counts when the laser was turned off. These tests confirmed that the detected signal is due only to the fluorescence of Rh6G induced by 1064 nm photon pairs.

Figure 3 shows the measurements of the fluorescence R_{fl} rate for three different Rh6G concentrations, $C = \{110 \text{ mmol/l}, 4.5 \text{ mmol/l}, 38 \text{ } \mu\text{mol/l}\}$ as a function of the number of SPDC pairs sent to the sample. These ETPA-induced fluorescence measurements with Rh6G clearly
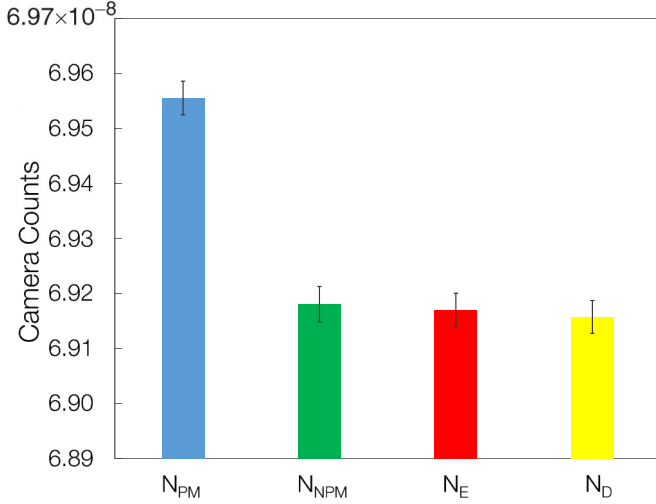
FIG. 2. Contributions to the detected photon count rate signal. N_{PM}: Raw ETPA-induced fluorescence for a 110 mmol/l Rh6G ethanol solution with 1W of pump power. N_{NPM}: Nonphase matching condition, PPLN crystal temperature decreased below that for degenerate SPDC. N_E: Cuvette with pure ethanol, no Rh6G in cuvette. N_D: The laser was turned off and there were no photons incident on the sample. Each result is an average of 10 measurements of 300 s Error bars (in all figures) are standard deviations over the set of measurements.

demonstrate a linear dependence of the fluorescence rate on the photon-pair rate. The pump power was varied over 0.25–1.5 W, which corresponds to 10^8–10^9 pairs per second sent to the Rh6G solution through the fiber. However, taking into account the dispersion in the fiber (2 m, connecting source and sample) and the width of the down-converted spectrum, only 10% of the overall SPDC rate, corresponding to 1063–1065 nm range, arrived within the (140 fs) coherence time
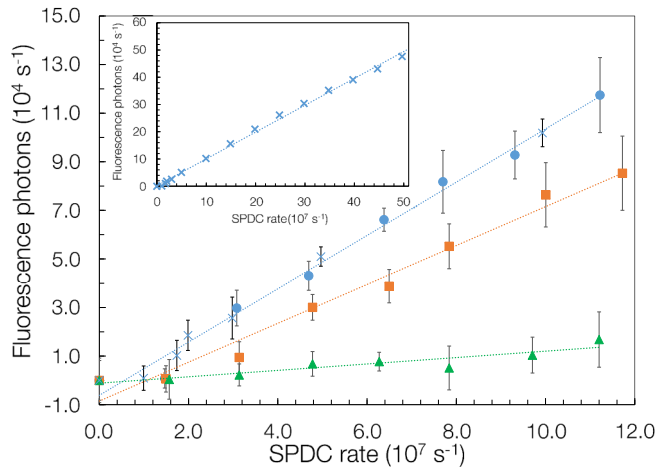

FIG. 3. ETPA-induced fluorescence rate as a function of the SPDC photon-pair rate for different Rh6G concentrations in ethanol: 110 mmol/l (blue circles), 4.5 mmol/l (orange squares), and 38 μmol/l (green triangles). A supplementary measurement (blue crosses) uses a free-space setup at 110 mmol/l allowing for higher rate (inset). Each point is an average of 10 measurements of 300 s.

TABLE I. Results for the ETPA cross section for two different Rh6G concentrations.

C [mmol/l]	σ_e [cm^2]
4.5	$(9.9 \pm 4.9) \times 10^{-22}$
0.038	$(1.9 \pm 0.9) \times 10^{-21}$

of the SPDC two-photon wave-packet. Thus, the effective photon-pair rate incident to the Rh6G solution varies from 2.0×10^7 to 1.2×10^8 s^{-1}.

The measured fluorescence rate R_{fl} can be described by

$$R_{fl} = \frac{N_{PM} - N_E}{t_{exp}} \frac{G}{\eta_{coll} \eta_{cam}}, \tag{1}$$

where t_{exp} is the integration time and the fluorescence rate is weighted by the gain factor of the camera G, the collection efficiency η_{col}, and the camera quantum efficiency η_{cam}.

Assuming the photon pair rate is undepleted, the ETPA and fluorescence rates are related through the quantum yield Y that is concentration- and solvent-dependent [8]:

$$R_{fl} = Y R_{abs} = Y C V N_A \sigma_e \phi_{pair}. \tag{2}$$

Here, C [mol/l] is the concentration, $V = 5.6 \times 10^{-9}$ l is the active volume, N_A is Avogadro's number, and $\sigma_e \phi_{pair} = R_e$ is the ETPA absorption rate per molecule.

In Eq. (1), the factors G, η_{col} and η_{cam} are difficult to quantify individually. We therefore determined them from a relative measurement with the 532 nm pump laser for SPA and estimate them all together. To do this, we sent the 532 nm pump laser through the system and replaced the long-pass filters IF$_H$ with a short-pass filter (Thorlabs FESH0650). The pump beam was attenuated to SPDC-intensity levels, such that 10^8 photons per second were focused in the cuvette. We then use Eq. (1), Eq. (2), and our knowledge of the SPA cross section to determine $G/(\eta_{coll} \eta_{cam}) = 4.5 \pm 0.9$ (counts)$^{-1}$.

Table I shows the values obtained for σ_e for low concentrations, where the quantum yield $Y = 0.95$ is known for Rh6G in an ethanol solution [21]. This would suggest values of $\sigma_e \sim 10^{-21}$ cm^2, which can be compared to SPA cross sections of around 10^{-17} cm^2 and TPA of around 10^{-47} cm^4 s [14]. A value of the yield for concentrations of 110 mmol/l in ethanol is not available, to the best of our knowledge, so we can report only the product, $Y\sigma_e = (6.4 \pm 0.5) \times 10^{-23}$ cm^2. This clearly demonstrates a significant quantum advantage with respect to the necessary photon fluxes compared to the TPA cross section. While these, and the following interferometric, measurements were more practical in fiber, we performed one series in free space. These results (crossed points in Fig. 3 and inset) match well with the fiber-based measurements but also provide a higher pair rate (losses due to dispersion were negligible).

The free-space measurement also allows us test the influence on the ETPA of the uncertainty in the photon pairs' spatial correlations, e.g., with respect to the concept of "entanglement area" [4]. In both the free-space and fiber configurations the whole focal spot is inside the sample, thus all pairs—spatially correlated or not, respectively—have a
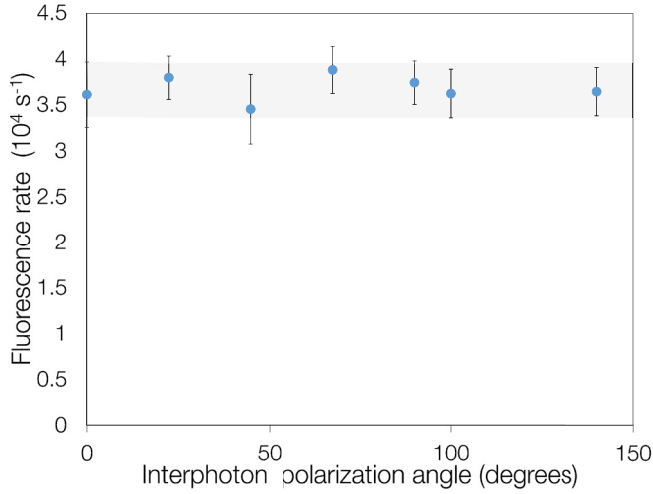
FIG. 4. Polarization dependence of ETPA-induced fluorescence rate for a 110 mmol/l Rh6G ethanol solution and an SPDC pair rate of 4.2×10^7 pairs/s as a function of the relative angle between the polarization of photons exiting from each arm. Each point is an average of 15 measurements of 300 s.

chance of interaction with a Rh6G molecule. The similarity of the results for both geometries indicate no such dependence.

IV. ETPA POLARIZATION AND TEMPORAL DEPENDENCE

To investigate the dependence of ETPA-induced fluorescence on the polarization of the pairs, we rotated the $\lambda/4$ waveplate in one of the interferometer arms [Fig. 1(c)]. As the photons probabilistically take either the same or different paths in the interferometer, we change the two-photon state from $|HH\rangle$ to a (50:50) mixture of states with orthogonal and parallel polarizations. In the case where photons separate and have the same polarization, there will be interference, which will cause rapid fluctuations; however, these will be averaged over due to the long integration times. Nonetheless, the mean photon pair rate sent to the cuvette remains constant as the polarization is rotated. Figure 4 shows the resulting fluorescence rate as a function of the polarization angle where the values vary by less than 10% indicating that there is no significant variation in the fluorescence due to the polarization state of the input photons. This is expected, as molecules in solution should not be polarized in the absence of magnetic fields or high molecular structure asymmetry.

A simple way to test the role of energy-time correlations of the photons arriving to the unit of absorbing media on the ETPA rate is to vary the time delay between the photons on the scale of their coherence time [see Fig. 1(c)]. Figure 5 shows the fluorescence rate as a function of the time delay between photons from an entangled pair for a fixed Rh6G concentration and photon-pair flux. The solid line is a Gaussian fit with a full width at half maximum of approximately 140 fs, which corresponds to the coherence time of the photon pairs. The small nonzero experimental background is due to photons that take the same path in the interferometer and hence do not have any time delay dependence, and the "shoulders" are from pairs
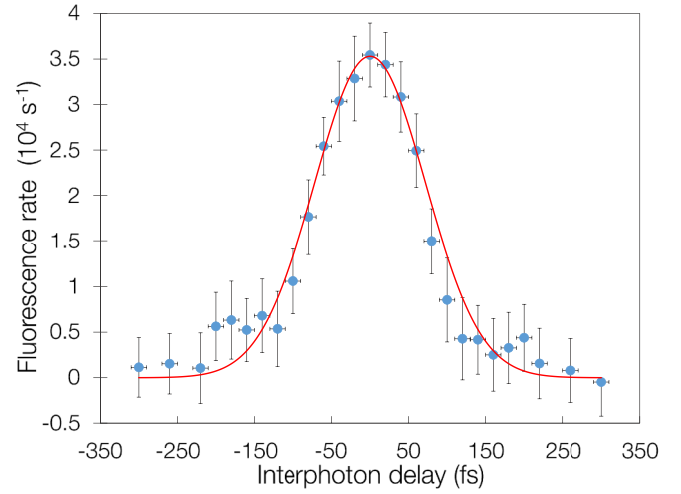

FIG. 5. Temporal dependence of ETPA-induced fluorescence rate for a 110 mmol/l Rh6G ethanol solution and an SPDC pair rate of 4.2×10^7 pairs/s, as a function of the interphoton delay $\Delta\tau$. The interferometer arm was scanned in 20 fs steps, and each point is an average of 15 measurements of 300 s. The solid line corresponds to a Gaussian fit with a FWHM $\sim$140 fs.

that have their (fiber) dispersion canceled by the time delay. In principle this background should be half the maximum; however, here it drops almost to the noise level. This drop is due to a lower than expected fluorescence signal at low input pair rates, especially for high concentrations (see Fig. 3). This drop is consistently reproducible, but further study is required to understand its origins.

V. CONCLUSION

We have performed a detailed study of ETPA in a molecular solution of Rh6G in ethanol and extracted values for the ETPA cross section, which shows a concentration-dependent response similar to [8]. We demonstrated the main signature of ETPA, i.e., a linear dependence of the absorption rate with the photon-pair rate for both open-space and fiber-coupled geometries. The similarity in these geometries indicated that the spatial correlations related to entanglement area do not play a role in the experimentally relevant case, i.e., beyond the single molecule approximation [4]. Also, as expected, there was no apparent dependence on the polarization of the photons probing the sample. Finally, we demonstrated a strong dependence of the signal on the interphoton delay that reflects the coherence time of the entangled two-photon wave packet. This can be seen as a fs-sensitive coincidence scheme, analogous to a Hong-Ou-Mandel experiment [22], revealing the form of the wave packet and a strong indicator that it is the energy-time entanglement that plays a fundamental role in ETPA.

[1] R. W. Boyd, *Nonlinear Optics* (Elsevier, New York, 2003).

[2] H. B. Bebb and A. Gold, Phys. Rev. **143**, 1 (1966).

[3] B. Mollow, Phys. Rev. **175**, 1555 (1968).

[4] H.-B. Fei, B. M. Jost, S. Popescu, B. E. A. Saleh, and M. C. Teich, Phys. Rev. Lett. **78**, 1679 (1997).

[5] B. Dayan, Phys. Rev. A **76**, 043813 (2007).

[6] F. Schlawin, J. Phys. B **50**, 203001 (2017).

[7] K. E. Dorfman, F. Schlawin, and S. Mukamel, Rev. Mod. Phys. **88**, 045008 (2016).

[8] J. P. Villabona-Monsalve, O. Calderon-Losada, M. Nuñez Portela, and A. Valencia, J. Phys. Chem. A **121**, 7869 (2017).

[9] D.-I. Lee and T. Goodson, J. Phys. Chem. B **110**, 25582 (2006).

[10] D.-I. Lee and T. Goodson, Proc. SPIE Lin. Nonlin. Opt. Org. Mat. VII **6653** (2007).

[11] M. R. Harpham, O. Süzer, C.-Q. Ma, P. Bäuerle, and T. Goodson, III, J. Am. Chem. Soc. **131**, 973 (2009).

[12] L. Upton, M. Harpham, O. Suzer, M. Richter, S. Mukamel, and T. Goodson, III, J. Phys. Chem. Lett. **4**, 2046 (2013).

[13] O. Varnavski, B. Pinsky, and T. Goodson, III, J. Phys. Chem. Lett. **8**, 388 (2017).

[14] P. Sperber and A. Penzkofer, Opt. Quantum Electron. **18**, 381 (1986).

[15] A. R. Guzman, M. R. Harpham, Ö. Süzer, M. M. Haley, and T. Goodson, III, J. Am. Chem. Soc. **132**, 7840 (2010).

[16] B. Dayan, A. Pe'er, A. A. Friesem, and Y. Silberberg, Phys. Rev. Lett. **93**, 023005 (2004).

[17] B. Dayan, A. Pe'er, A. A. Friesem, and Y. Silberberg, Phys. Rev. Lett. **94**, 043602 (2005).

[18] A. Pe'er, B. Dayan, A. A. Friesem, and Y. Silberberg, Phys. Rev. Lett. **94**, 073601 (2005).

[19] J. D. Franson, Phys. Rev. Lett. **62**, 2205 (1989).

[20] A. R. Guzman, M. R. Harpham, Ö. Süzer, and T. G. Goodson, III, Proc. SPIE Lin. Nonlin. Opt. Org. Mat. X **7774** (2010).

[21] R. F. Kubin and A. N. Fletcher, J. Lumin. **27**, 455 (1982).

[22] C.-K. Hong, Z.-Y. Ou, and L. Mandel, Phys. Rev. Lett. **59**, 2044 (1987).